AGU PUBLICATIONS

Geophysical Research Letters

RESEARCH LETTER
10.1002/2014GL059510

Key Points:
- Local parameterization of the MDT in the North Atlantic Ocean
- Associated covariance matrix tailored to the integration into ocean models
- The contribution of GOCE to the MDT and the progress done in GOCE processing

Correspondence to:
S. Becker,
silvia.becker@uni-bonn.de

Citation:
Becker, S., J. M. Brockmann, and W.-D. Schuh (2014), Mean dynamic topography estimates purely based on GOCE gravity field models and altimetry, *Geophys. Res. Lett.*, *41*, 2063–2069, doi:10.1002/2014GL059510.

Received 4 FEB 2014
Accepted 26 FEB 2014
Accepted article online 3 MAR 2014
Published online 19 MAR 2014

Mean dynamic topography estimates purely based on GOCE gravity field models and altimetry

S. Becker[1], J. M. Brockmann[1], and W.-D. Schuh[1]

[1] Department of Theoretical Geodesy, Institute of Geodesy and Geoinformation, University of Bonn, Bonn, Germany

Abstract The quality of mean dynamic topography (MDT) models derived from an altimetric mean sea surface and a gravity field model mainly depends on the spatial resolution and accuracy of the particular gravity field model. We use an integrated approach which allows for estimating the MDT and its (inverse) covariance matrix on a predefined grid which is one of the requirements for ocean data assimilation. The quality and accuracy of the MDT directly reflects the quality and accuracy of the used gravity field model. For the first time, MDT estimates along with its full error covariance matrix based on Gravity Field and Steady-State Ocean Circulation Explorer (GOCE) data can be provided. We demonstrate the progress accomplished with GOCE processing and the valuable contribution of the GOCE gravity field models regarding the estimation of the MDT by showing results based on altimetric observations of Jason-1 and Envisat in combination with different GOCE gravity field models for the North Atlantic.

1. Introduction

The European Space Agency (ESA) satellite mission GOCE (Gravity Field and Steady-State Ocean Circulation Explorer) was launched in March 2009 and completed its mission in October 2013. The mission's main objective was to map the Earth's gravity field and accordingly the geoid with a spatial resolution of approximately 100 km at centimeter accuracy. Its second mission goal as an ocean circulation explorer is closely related to this task. The ocean's dynamic topography as the difference between the sea surface and the geoid reflects many characteristics of the ocean circulation. Consequently, the accurate knowledge of the geoid is essential for the computation of the dynamic topography and the deduced geostrophic velocities, which are proportional to the gradients of the mean dynamic topography. Due to the unprecedented accuracy and spatial resolution of satellite-based, altimeter-independent gravity field models provided with GOCE, these models have great impact on ocean current estimations and greatly improve the understanding of the ocean circulation.

Unfortunately, the computation of the dynamic topography is not straightforward because of the different representations and spatial resolutions of the involved data sets. Satellite-based gravity field models are usually represented by a band-limited series of global spherical harmonic functions. The accuracies of the estimated spherical harmonic coefficients decrease with increasing degree due to the unfavorable signal-to-noise ratio for high frequencies at satellite altitude. In contrast to the geoid, the sea surface can be directly observed by satellite altimetry. Several satellite altimeters provide measurements of the sea surface height with superior accuracy and spatial resolution since the 1970s.

Existing studies regarding dynamic topography and ocean circulation estimates from GOCE [e.g., *Knudsen et al.*, 2011; *Bingham et al.*, 2011; *Albertella et al.*, 2012; *Janjić et al.*, 2012] as well as pre-GOCE studies [e.g., *Andersen and Knudsen*, 2009; *Maximenko et al.*, 2009; *Rio et al.*, 2011] make use of special filter techniques to homogenize the different information and to combine a gravity field model with altimetric-derived sea surface heights. No or only insufficient information about the variances and especially the covariances are provided with these dynamic topography models. Within our approach [see, e.g., *Becker et al.*, 2012; *Becker*, 2012], full covariance matrices of all data sets are considered accounting for instrumental errors as well as omission errors in order to estimate the dynamic topography and its covariance matrix. Consequently, a straightforward evaluation and validation of the GOCE gravity field models is possible. Meanwhile, there are four releases of the GOCE gravity field models available. We use those derived by the time-wise approach as these models are purely based on GOCE data.

Table 1. Overview Over Different GOCE Gravity Field Models

Model Name	Maximum Spherical Harmonic d/o n_{max}	Days of Data	Accuracy of Geoid for d/o 180 (111 km)
TIM01	224	71	7.2 cm
TIM02	250	225	4.1 cm
TIM03	250	362	3.2 cm
TIM04	250	806	2.0 cm

The paper is organized as follows. Section 2 summarizes the data types used in this study. The applied method to estimate the ocean's dynamic topography is outlined in section 3. The results obtained with the different GOCE gravity field models are presented in section 4. The paper closes with a discussion in section 5.

2. Data Types

2.1. GOCE Gravity Field Models

In this study, we use the full normal equations of the releases 1–4 of the GOCE gravity field models following the time-wise approach [*Pail et al.*, 2011; *Brockmann et al.*, 2013], denoted as TIM01–TIM04 in the following. Table 1 gives an overview over the different models regarding the maximum degree n_{max} of the spherical harmonic expansion, the number of days of data used for the particular computations and the accuracy expressed in geoid heights corresponding to degree and order 180 (equivalent to a spatial resolution of 111 km or 1° representing approximately GOCE's mission goal of a centimeter geoid).

2.2. Altimetric Mean Sea Surface

A combined mean sea surface height profile for the North Atlantic Ocean was derived from Jason-1 and Envisat sea surface height measurements provided by Archiving, Validation, and Interpretation of Satellite Oceanographic data (http://www.aviso.oceanobs.com). We used monomission along-track data sets reduced by geophysical and range corrections for the time period between October 2002 (first available data of Envisat) and February 2009 (orbit change of Jason-1). A rigorous variance propagation was implemented during the necessary processing steps based on empirical covariance functions along the satellite tracks. As a result, we obtained the full covariance matrix of the mean sea surface height profile in order to build the altimetric normal equations. Details of the processing steps concerning the altimetric data are found in *Becker* [2012] and *Becker et al.* [2013].

3. Combination Method

The mean dynamic topography (MDT) models shown below are derived by applying the rigorous combination method described in detail by *Becker et al.* [2012] and *Becker* [2012]. The geoid and the MDT are assessed simultaneously. The geoid is parameterized by spherical harmonics as usual. The maximum degree of the spherical harmonics expansion is set to $\bar{n}_{max} = 360$ for all results shown in this study. The MDT is represented by a linear combination of local finite element basis functions. Here we use two-dimensional linear piecewise polynomials as basis functions so that the unknowns are directly the MDT at the nodal points which are located on a triangulated 1° × 1° grid over the North Atlantic (4.5°–78.5°N, 19.5°–97.5°W). This specific MDT parameterization corresponds to a spatial resolution of a spherical harmonics expansion up to degree and order 180 at which GOCE's mission goal is to provide the geoid with centimeter accuracy. The altimetric mean sea surface is now considered as the sum of geoid and MDT. In addition, we introduce smoothness conditions in terms of a regularization for the high-frequency gravity field parameters according to the Hilbert Space H^1_Γ [*Schuh and Becker*, 2010] for spherical harmonics of degree $180 \le n \le 360$ due to the lack of information content in this frequency domain. We use Kaula's rule of thumb [*Kaula*, 1966] as a priori information to constrain the size of the unknown gravity field coefficients. Furthermore, the omission domain is parameterized within the altimetric observation equations based on a priori information according to Kaula's rule using an isotropic homogeneous covariance function to accomplish a complete modeling of the observations.

Finally, the different observation groups are combined in terms of normal equations

$$\left(w_G \mathbf{N}_G + w_{MSS} \mathbf{N}_{MSS} + w_R \mathbf{N}_R\right) \mathbf{x} = w_G \mathbf{n}_G + w_{MSS} \mathbf{n}_{MSS} \quad (1)$$

with the specific normal equation matrices $\mathbf{N}_{G,MSS,R}$ and right-hand side vectors $\mathbf{n}_{G,MSS}$ for the gravity field (G), the mean sea surface (MSS), and the smoothness conditions (R) or the regularization, respectively. The relative weights $w_{G,MSS,R}$ are determined by a rigorous variance component estimation [see, e.g., *Koch and Kusche*, 2002; *Brockmann and Schuh*, 2010] to estimate the gravity field ($\mathbf{x}_{cs}$) and MDT ($\mathbf{x}_{MDT}$) parameters contained in the vector $\mathbf{x} = \left[\, \mathbf{x}_{cs} \;\; \mathbf{x}_{MDT} \,\right]^T$. Overall, there are almost 135,000 unknown parameters which require the implementation in a high-performance computing environment.

The most challenging task is the separation of the altimetric mean sea surface into the geoid and the mean dynamic topography. If the spatial resolution of the finite elements matches the frequency domain of the gravity field model, which can be resolved with high accuracy, the combined model provides a smooth mean dynamic topography [*Becker*, 2012]; i.e., the altimetric mean sea surface can be separated very well. Otherwise, the estimated MDT begins to oscillate and reflects the high-frequency part of the included altimetric information. In either case, the characteristics of the estimated MDT are reflected by the model and the method yields a consistent error description. Consequently, the method is best suited for evaluating the particular gravity field model.

Note that the full (inverse) covariance matrix of the MDT results from the described procedure. The nodal points of the finite elements can be predefined by any ocean model grid so that the estimated MDT along with its (inverse) covariance matrix can be directly integrated into an ocean circulation model without any further processing steps. Integrating such a MDT model into a stationary inverse ocean model indicates the success of the approach [*Becker et al.*, 2012, 2013]. Because of the consistent covariance matrix, possible unphysical noise in the MDT is rejected by the ocean model.

The described method is tailored to the integration of a MDT model into ocean circulation models, in which the MDT along with its inverse covariance matrix is merged with the oceanographic information. Because no special filter technique or smoothness condition is explicitly applied to the MDT, the full signal content of the observations is contained in the estimated MDT. Smoothness is then implied by the inverse covariance matrix. If the MDT itself is to be used for further studies regarding, e.g., the geostrophic velocities without using directly the covariance matrix, smoothness conditions must be applied to the MDT. Within our model, mathematical constraints can optionally be added to the MDT parameters. The MDT ζ can be written in short as

$$\zeta = \mathbf{A}\mathbf{x}_{MDT} \tag{2}$$

with the matrix $\mathbf{A}$ containing the basis functions or functional relation, respectively. In order to obtain a smooth MDT, the norm of the gradient $|\nabla(\mathbf{A}\mathbf{x}_{MDT})|$ should be small. The gradient of the MDT can be expressed as

$$\boldsymbol{\nabla}\zeta = \boldsymbol{\nabla}(\mathbf{A}\mathbf{x}_{MDT}) = \begin{bmatrix} \mathbf{A}_x \\ \mathbf{A}_y \end{bmatrix} \mathbf{x}_{MDT} = \begin{bmatrix} \mathbf{0} & \mathbf{A}_x \\ \mathbf{0} & \mathbf{A}_y \end{bmatrix} \begin{bmatrix} \mathbf{x}_{cs} \\ \mathbf{x}_{MDT} \end{bmatrix} \tag{3}$$

with the matrices $\mathbf{A}_x$ and $\mathbf{A}_y$ containing the derivatives of the basis functions in local east and north, respectively. Instead of minimizing the weighted squared sum of the residuals $v_{G,MSS,R}$

$$\Phi = w_G \mathbf{v}_G^T \mathbf{P}_G \mathbf{v}_G + w_{MSS} \mathbf{v}_{MSS}^T \mathbf{P}_{MSS} \mathbf{v}_{MSS} + w_R \mathbf{v}_R^T \mathbf{P}_R \mathbf{v}_R \tag{4}$$

with the inverse covariance matrices $\mathbf{P}_{G,MSS,R}$ of the different observation groups, the following equation must be minimized to obtain a small gradient

$$\overline{\Phi} = \Phi + w_S (\boldsymbol{\nabla}\zeta)^T (\boldsymbol{\nabla}\zeta) \tag{5}$$

with the weight w_S defining the impact of the additional constraints on the solution, which is also determined by variance component estimation. Equation (5) can also be considered as an optimization problem with the side constraint of a minimum squared norm of the gradient with w_S denoting the Lagrange multiplier. To solve this problem, the normal equations (1) are consequently extended by one component. The additional normal equation matrix follows from

$$\mathbf{N}_S = \begin{bmatrix} \mathbf{0} & \mathbf{0} \\ \mathbf{A}_x^T & \mathbf{A}_y^T \end{bmatrix} \begin{bmatrix} \mathbf{0} & \mathbf{A}_x \\ \mathbf{0} & \mathbf{A}_y \end{bmatrix} = \begin{bmatrix} \mathbf{0} & \mathbf{0} \\ \mathbf{0} & \mathbf{A}_x^T \mathbf{A}_x + \mathbf{A}_y^T \mathbf{A}_y \end{bmatrix} \tag{6}$$

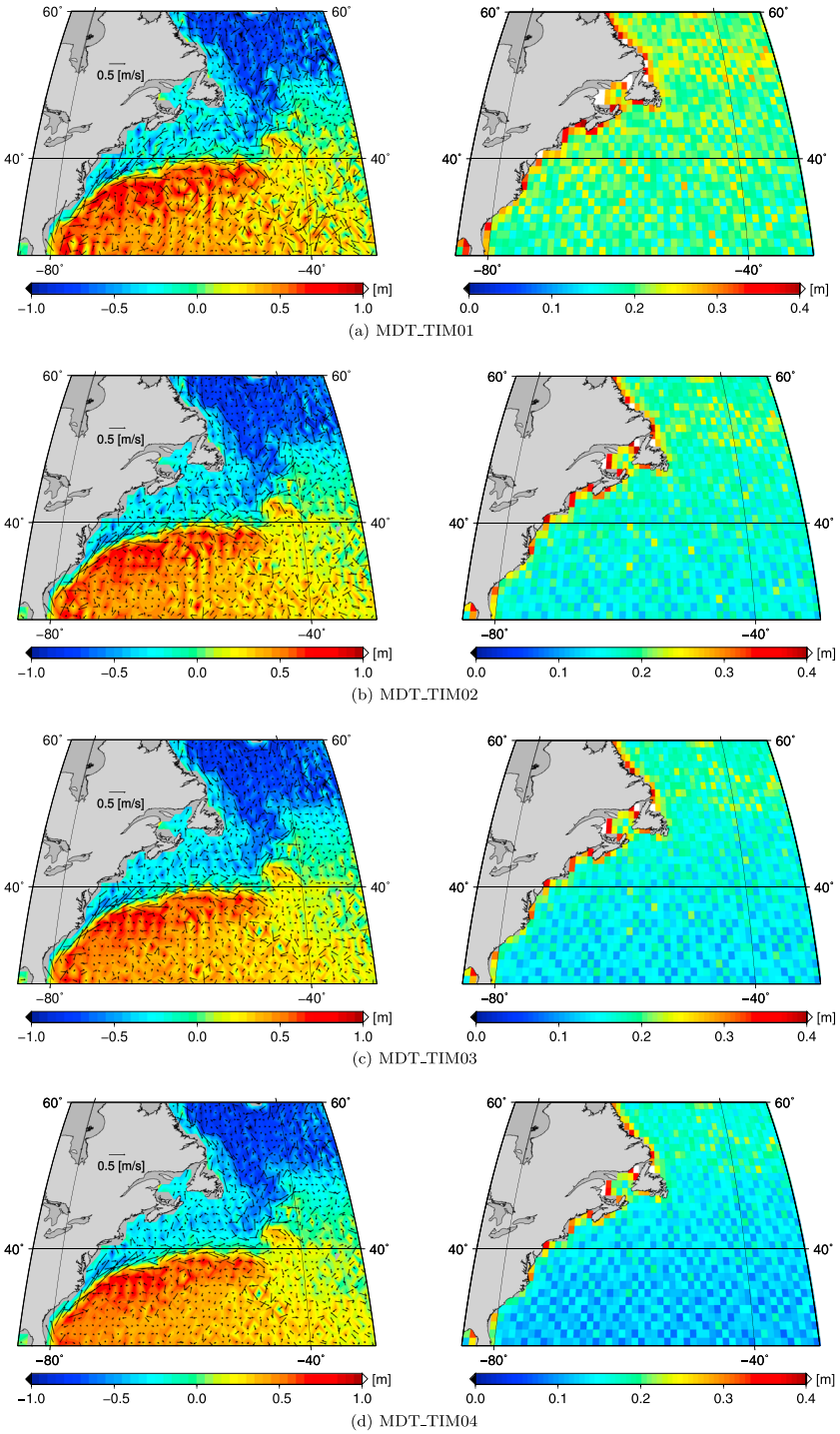

Figure 1. (left) Estimated mean dynamic topography with derived geostrophic velocities based on the different GOCE gravity field models within a section of the North Atlantic Ocean. (right) Corresponding standard deviations of the different mean dynamic topography estimates.

and the overall normal equations can be written as

$$\left(w_G\mathbf{N}_G + w_{MSS}\mathbf{N}_{MSS} + w_R\mathbf{N}_R + w_S\mathbf{N}_S\right)\mathbf{x} = w_G\mathbf{n}_G + w_{MSS}\mathbf{n}_{MSS} \tag{7}$$

Note that in case of a regular grid with equidistant nodal points and linear polynomials as base functions, the discrete Laplace operator follows for inner nodal points as entries in $\mathbf{N}_S$.

Table 2. Mean Standard Deviations of the Estimated MDT Models σ_{MDT}, RMS of the MDT Signal and Comparisons to Other MDT Models for the Overall Study Area Over the North Atlantic Ocean

			RMS of Differences (m)			Scaled MAD of Differences M_I(m)			Scaled MAD of Relative Difference R_I		
Model Name	Mean σ_{MDT}(m)	RMS of Signal (m)	CLS09	DTU10	Niiler	CLS09	DTU10	Niiler	CLS09	DTU10	Niiler
MDT_TIM01	0.211	0.445	0.234	0.225	0.222	0.183	0.182	0.182	0.922	0.907	0.918
MDT_TIM02	0.182	0.430	0.204	0.193	0.192	0.159	0.156	0.156	0.938	0.910	0.923
MDT_TIM03	0.169	0.423	0.189	0.178	0.176	0.145	0.142	0.144	0.940	0.919	0.926
MDT_TIM04	0.151	0.416	0.175	0.163	0.162	0.127	0.123	0.129	0.921	0.911	0.944
MDT_TIM04S	0.048	0.388	0.077	0.054	0.066	0.048	0.041	0.049	1.027	0.865	1.054
CLS09	—	0.394	—	0.081	0.078	—	0.038	0.029	—	—	—
DTU10	—	0.375	—	—	0.052	—	—	0.038	—	—	—
Niiler	—	0.381	—	—	—	—	—	—	—	—	—

4. Discussion of Results

Figure 1 shows the resulting mean dynamic topography models, denoted as MDT_TIM01–MDT_TIM04, and the deduced geostrophic velocities based on the different GOCE gravity field models TIM01–TIM04 without any additional smoothness constraints applied to the MDT parameters. In order to provide a deeper insight into the results, we only show a section of our study area in the North Atlantic Ocean centered on the Gulf Stream. The visible unphysical oscillations of the estimated MDT imply insufficient accurate gravity field information at this specific grid resolution of $1°\times1°$ corresponding to a spherical harmonics expansion up to degree and order 180 (cf. Table 1). However, the progress and improvements made starting from the TIM01 to the TIM04 model can clearly be observed. The oscillations decrease, and the mean dynamic topography gets smoother. Consequently, the derived geostrophic velocities marked by the arrows become less random but more physically motivated clearly showing proof of the enhancement of the GOCE gravity field models.

This is also reflected by the corresponding error estimates of the mean dynamic topography, also illustrated in Figure 1. For all GOCE gravity field models, the errors are largest at the coastlines where the separation of the altimetric mean sea surface into geoid and mean dynamic topography is most challenging. Overall, the standard deviations decrease comparing the results for the TIM01 to TIM04 model which is consistent with the characteristics of the particular MDT itself.

Table 2 summarizes the averaged standard deviations σ_{MDT}, the root-mean-square (RMS) of the MDT signal for the different solutions, and comparison findings to three other MDT estimates, namely, the CLS09 [*Rio et al.*, 2011], DTU10 [*Andersen and Knudsen*, 2009], and Niiler [*Maximenko et al.*, 2009] mean dynamic topography model. Note that these results refer to the overall study area over the North Atlantic Ocean between 4.5°–78.5°N and 19.5°–97.5°W.

The mean standard deviation as well as the signal RMS decrease in the progress of the four GOCE gravity field models from ≈ 21 cm to ≈ 15 cm and from ≈ 44 cm to ≈ 41 cm, respectively. The RMS of the MDT signal still remains larger than the signal RMS values of the comparison models which are also listed in Table 2 possibly reflecting the roughness of the estimated MDT.

To evaluate the model agreement, we additionally show the particular RMS of the differences between our results and the three comparison models, the scaled median of absolute deviation (MAD = median ($|x_i - \text{median}(x_i)|$)) [*Huber*, 1981, see chapter 5, pp. 107–108] of the differences as a robust estimation of the standard deviation

$$M_I = 1.4826\text{MAD}(\text{MDT\_TIM0X}_i - \text{MDT\_}I_i), \tag{8}$$

and the scaled MAD of the differences normalized by the respective error estimation

$$R_I = 1.4826\text{MAD}\left(\frac{\text{MDT\_TIM0X}_i - \text{MDT\_}I_i}{\sigma_{\text{MDT}_i}}\right) \tag{9}$$

with MDT_TIM0X denoting our estimates and $I \in$ (CLS09, DTU10, or Niiler). The factor 1.4826 accounts for making MAD consistent at the normal distribution. The specific results are also given in Table 2. In general, the RMS values of the differences decrease for all comparison models looking at the different solutions;

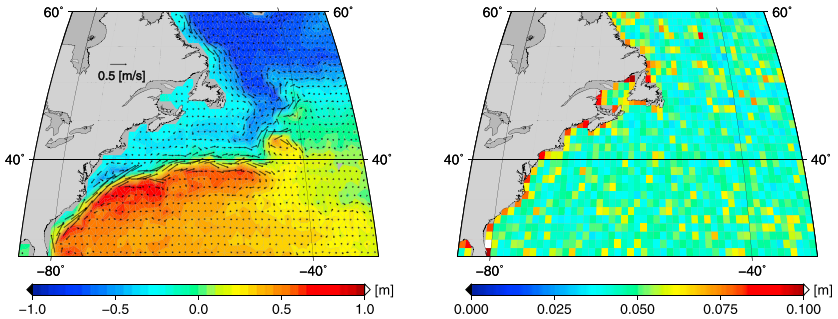

Figure 2. Mean dynamic topography model MDT_TIM04S and associated standard deviations based on the TIM04 gravity field model with additional smoothness conditions applied to the MDT parameters.

i.e., the model agreement gets better. While the RMS for the CLS09 model is always the largest, the one for the Niiler model is the smallest in either case. The scaled MAD of the differences M_I also decreases in the progress of the GOCE models. The smallest value is obtained with the DTU10 model. This circumstance is also reflected by the scaled MAD of the normalized differences R_I. The smallest R_I results from the DTU10 model. R_I is always smaller than 1 and remains at the same order of magnitude, which implies consistency of the error estimates and the MDT characteristics regarding unphysical oscillations. Overall, the largest differences can be observed with all comparison models around Cuba, along the Gulf Stream, and, as expected, at the coastlines or the boundaries, respectively.

Figure 2 shows the mean dynamic topography with the geostrophic velocities and the corresponding standard deviations resulting from the TIM04 gravity field model and additional smoothness conditions for the MDT (cf. section 3 and equations (5)–(7)), denoted as MDT_TIM04S. The respective results regarding the mean standard deviation, the signal RMS, and comparisons to the external models are also listed in Table 2. Due to the added constraints, the separation of the altimetric mean sea surface into geoid and MDT is facilitated and the error estimates remarkably decrease to $\approx$ 5 cm on average. The RMS of the MDT signal decreases again and lies now between those of the comparison models. The RMS values of the differences also considerably decrease. In contrast to the unfiltered results, the differences to the DTU10 model show the smallest RMS. The MAD of the differences M_I decreases as well and is the smallest with the DTU10 model, which also results in the smallest MAD of relative differences R_I. This slightly decreases in comparison to the MDT models without additional smoothness conditions while the corresponding values of the other models increase to >1, although the particular RMS of the differences and M_I decreases. Note that an increased value of R_I implies that the standard deviations σ_{MDT_i} show a stronger decrease than the differences, and vice versa. Again, the largest differences can be observed in the Caribbean Sea and along the Gulf Stream.

In summary, our MDT estimates mostly agree with the comparison models within the corresponding error estimate. The best agreement can generally be observed with the DTU10 model which becomes most evident with the MDT_TIM04S model. However, the three models are obviously not error free. In fact, these errors also need to be taken into account to accomplish an objective comparison. In addition, all models are based on different data sources which makes a comparison even more difficult. Note in this context that both the CLS09 and the Niiler model are additionally based on in situ data in contrast to the DTU10 and our models so that the largest differences can be expected with those models. For the sake of completeness, the disagreement between the individual comparison models is demonstrated in terms of the RMS of the differences and the scaled MAD of the individual differences in Table 2.

5. Conclusions

We showed MDT estimates resulting from a rigorous method combining gravity field information with altimetric measurements in a consistent way accounting for both instrumental and omission errors. The quality of the resulting mean dynamic topography depends on the used gravity field model in combination with the resolution of the target grid. Potentially, noise in the MDT signal field is caused by insufficiently accurate gravity field information on the particular grid. However, the noise is consistently reflected by the full covariance matrix. The MDT and the covariance matrix must be used in combination; e.g., the MDT and its inverse covariance matrix as weight matrix can be directly integrated into an ocean circulation model as the

finite element grid can be predefined by the nodal points of the ocean model. Furthermore, we can optionally apply additional smoothness conditions explicitly to the MDT parameters providing a smooth MDT for a direct analysis.

GOCE gravity field models strongly contribute to improving the estimation of the MDT, which can be confirmed by comparisons to computations based only on a GRACE gravity field model [*Becker*, 2012]. Experiments using a combined GRACE/GOCE gravity field model showed that including the additional information of a GRACE gravity field model hardly changes the results; its contribution is negligibly small. The great advantage of a GOCE gravity field model compared to a GRACE gravity field model regarding ocean circulation estimates becomes apparent.

Using the different GOCE gravity field models reveals the progress made from the first GOCE gravity field release to the current one. During its last mission phase, GOCE's orbit was lowered to obtain even better results. Consequently, the final fifth release of GOCE gravity field models planned for mid-2014 is very promising.

Acknowledgments

This work was funded within the DFG priority program SPP 1257 "Mass transport and mass distribution in the system Earth," the DFG project G/O2000+, and the project COSIMO within ESA's Support To Science Element program. The computations were performed on the JUROPA supercomputer at FZ Jülich. The computing time was granted by John von Neumann Institute for Computing (project HBN15).

The Editor thanks Ole B. Andersen and an anonymous reviewer for their assistance in evaluating this paper.

References

Albertella, A., R. Savcenko, T. Janjić, R. Rummel, W. Bosch, and J. Schröter (2012), High resolution dynamic ocean topography in the Southern Ocean from GOCE, *Geophys. J. Int.*, *190*, 922–930, doi:10.1111/j.1365-246X.2012.05531.x.

Andersen, O., and P. Knudsen (2009), DNSC08 mean sea surface and mean dynamic topography models, *J. Geophys. Res.*, *114*, C11001, doi:10.1029/2008JC005179.

Becker, S. (2012), Konsistente Kombination von Schwerefeld, Altimetrie und hydrographischen Daten zur Modellierung der dynamischen Ozeantopographie, Universität Bonn. [Available at http://hss.ulb.uni-bonn.de/2012/2919/2919.htm.]

Becker, S., G. Freiwald, M. Losch, and W.-D. Schuh (2012), Rigorous fusion of gravity field, altimetry and stationary ocean models, *J. Geodyn.*, *59–60*, 99–110, doi:10.1016/j.jog.2011.07.0069.

Becker, S., M. Losch, J. Brockmann, G. Freiwald, and W.-D. Schuh (2013), A tailored computation of the mean dynamic topography for a consistent integration into ocean circulation models, *Surv. Geophys.*, doi:10.1007/s10712-013-9272-9, in press.

Bingham, R. J., P. Knudsen, O. Andersen, and R. Pail (2011), An initial estimate of the North Atlantic steady-state geostrophic circulation from GOCE, *Geophys. Res. Lett.*, *38*, L01606, doi:10.1029/2010GL045633.

Brockmann, J., E. Höck, I. Krasbutter, T. Mayer-Guerr, R. Pail, W.-D. Schuh, and N. Zehentner (2013), Performance of the fourth generation GOCE time-wise Earth gravity field model, presented at the 2013 General Assembly of the European Geosciences Union, Vienna, Austria, April 07–12 (EGU2013-9401).

Brockmann, J.-M., and W.-D. Schuh (2010), Fast variance component estimation in GOCE data processing, in *Gravity, Geoid and Earth Observation, IAG Symposia*, edited by S. Mertikas, pp. 185–193, Springer, Berlin, Heidelberg. doi:10.1007/978-3-642-10634-7_25.

Huber, P. (1981), *Robust Statistics*, John Wiley, New York-Chichester-Brisbane-Toronto.

Janjić, T., J. Schröter, R. Savcenko, W. Bosch, A. Albertella, R. Rummel, and O. Klatt (2012), Impact of combining GRACE and GOCE gravity data on ocean circulation estimates, *Ocean Sci.*, *8*(1), 65–79, doi:10.5194/os-8-65-2012.

Kaula, W. M. (1966), *Theory of Satellite Geodesy*, Blaisdell Publ. Co., Waltham, Mass.-Toronto-London.

Knudsen, P., R. Bingham, O. Andersen, and M.-H. Rio (2011), A global mean dynamic topography and ocean circulation estimation using a preliminary GOCE gravity model, *J. Geod.*, *85*, 861–879, doi:10.1007/s00190-011-0485-8.

Koch, K. R., and J. Kusche (2002), Regularization of geopotential determination from satellite data by variance components, *J. Geod.*, *76*, 259–268, doi:10.1007/s00190-002-0245-x.

Maximenko, N., P. Niiler, M.-H. Rio, O. Melnichenko, L. Centurioni, D. Chambers, V. Zlotnicki, and B. Galperin (2009), Mean dynamic topography of the ocean derived from satellite and drifting buoy data using three different techniques, *J. Atmos. Oceanic Technol.*, *26*, 1910–1918, doi:10.1175/2009JTECHO672.1.

Pail, R., et al. (2011), First GOCE gravity field models derived by three different approaches, *J. Geod.*, *85*(11), 819–843, doi:10.1007/s00190-011-0467-x.

Rio, M.-H., S. Guinehut, and G. Larnicol (2011), New CNES-CLS09 global mean dynamic topography computed from the combination of GRACE data, altimetry, and in situ measurements, *J. Geophys. Res.*, *116*, C07018, doi:10.1029/2010JC006505.

Schuh, W.-D., and S. Becker (2010), Potential field and smoothness conditions, in *The Apple of Knowledge—In Honour of Prof. N. Arabelos*, edited by M. Contadakis et al., pp. 237–250, University of Thessaloniki, AUTH - Faculty of Rural and Surveying Engineering, Thessaloniki, Greece.